Liquid film dynamics in horizontal and tilted tubes: dry spots and sliding drops

A.A. King,[1] L.J. Cummings,[1] S. Naire[2] & O.E. Jensen[1*]
[1]School of Mathematical Sciences, University Park,
University of Nottingham, Nottingham NG7 2RD, UK;
[2]School of Computing and Mathematics, University of Keele,
Staffordshire ST5 5BG, UK

February 12, 2007

Abstract

Using a model derived from lubrication theory, we consider the evolution of a thin viscous film coating the interior or exterior of a cylindrical tube. The flow is driven by surface tension and gravity and the liquid is assumed to wet the cylinder perfectly. When the tube is horizontal, we use large-time simulations to describe the bifurcation structure of the capillary equilibria appearing at low Bond number. We identify a new film configuration in which an isolated dry patch appears at the top of the tube and demonstrate hysteresis in the transition between rivulets and annular collars as the tube length is varied. For a tube tilted to the vertical, we show how a long initially uniform rivulet can break up first into isolated drops and then annular collars, which subsequently merge. We also show that the speed at which a localized drop moves down the base of a tilted tube is non-monotonic in tilt angle.

1 Introduction

A liquid film coating the interior or exterior of a cylindrical tube of circular cross-section can evolve under the action of surface tension, gravity and viscous forces to spatially non-uniform and time-dependent configurations of considerable complexity. Such films are of widespread practical importance, for example as industrial coatings or as the protective layer lining a lung airway, as well as being familiar through everyday experience (such as rain-drops on a washing line). As long as the film remains thin relative to the cylinder radius, so that the film's dynamics can be modeled using lubrication theory, and provided the film wets the cylinder's surface, so that the film does not rupture in finite time, the flow may be described by the spatially two-dimensional nonlinear evolution equation (2.1) below. In this paper we present numerical and asymptotic solutions of (2.1) demonstrating some key features of the film's dynamics, including a new equilibrium

*Email: Oliver.Jensen@nottingham.ac.uk

configuration for horizontal tubes and complex transient behavior in tubes that are tilted from the horizontal.

In the absence of gravity, surface tension γ acting on a thin wetting film coating a long cylinder of radius a causes the film (via the Plateau–Rayleigh instability) to assume a variety of quasi-static axisymmetric shapes, often termed collars and lobes. We use the term *collar* to denote a small-amplitude annular unduloid of length $2\pi a$ that wets the cylinder with zero effective contact angle; likewise an annular *lobe* has length less than $2\pi a$ and non-zero effective contact angle. Lobes and collars are connected by thin transition regions allowing fluid to drain slowly from lobe to collar, so that the film thickness is everywhere bounded away from zero. Hammond [1] showed how an initially uniform film on a cylinder of length greater than $2\pi a$ can evolve into collars and lobes that are stationary over long times (see also [2, 3]). More recently, Lister *et al.* [4] demonstrated that over even longer times, and for sufficiently long cylinders, collars can exhibit surprisingly intricate dynamics, periodically sweeping along the tube from one end to the other.

Such behavior is readily disrupted by gravity, even when the Bond number $\rho g a^2/\gamma$ is small (here ρ is the fluid density and g gravitational acceleration). Weak gravitational forcing causes a collar to move down a vertical tube, accumulating fluid at its leading edge and depositing it at its rear. A very slowly moving collar deposits a very thin trailing film, allowing the collar's volume to increase over time to the extent that solutions of (2.1) can exhibit finite-time blow-up; in practice, the film thickens so much that the thin-film assumption underlying lubrication theory is violated [5]. Multiple collars exhibit coarsening, with large collars traveling faster than smaller ones and subsequently merging with them; this also promotes blow-up [6]. Blow-up may be regularized by retaining the fully nonlinear expression for the interfacial curvature in the governing evolution equation. This captures the growth of a collar on the exterior of a tube into an isolated bead or drop [7, 8], or the growth and snap-off of a collar on the interior of a tube to form an occlusive liquid bridge [9, 10]. Beads or bridges form on vertical tubes only if the Bond number is sufficiently small; strong gravitational forcing suppresses the initial collar growth by saturating the primary Plateau–Rayleigh instability at small amplitudes [11, 12].

The flow of a liquid film on a horizontal tube is subject to two competing effects: gravity causes draining of the flow towards the base of the tube to form a rivulet, whereas surface tension, again acting through the Plateau–Rayleigh instability, seeks to cause the film to break up into collars or isolated drops. Asymptotic drainage rates during the formation of a rivulet were identified and analyzed by Jensen [13] in the mathematically equivalent problem of surface-tension-driven flow of a thin film on a weakly curved tube (see also [14, 15]); he also identified the solution structure of some of the nonaxisymmetric capillary equilibria that form at small Bond number (uniform or wavy rivulets, isolated drops or drops connected to their neighbors by thin rivulets). Weidner *et al.* [16], using simulations of an evolution equation similar to (2.1) that included higher-order corrections in film thickness, described the dynamic transition from a uniform film coating the exterior of a cylinder to a pendent rivulet, which became wavy before breaking up to form isolated pendent drops. These authors also described how a sufficiently thick film can form an equilibrium nonaxisymmetric collar (a drop that extends around to the top of the tube). At large Bond numbers the break-up of a pendent rivulet into drops can be regarded as a form of Rayleigh–Taylor instability. De Bruyn demonstrated experimentally the transition between Plateau–Rayleigh and Rayleigh–Taylor instabilities as the

Bond number is increased [17], with the transition occuring when the film thickness is comparable to the capillary length $(\gamma/\rho g)^{1/2}$. Duclaux *et al.* [18] identified experimentally a criterion relating Bond number to film thickness necessary for liquid lining the interior of a horizontal tube to snap-off to form an occlusive bridge.

In this paper we use time-dependent simulations and asymptotics to describe some solutions of (2.1) representing the evolution of a thin film coating either the inside or outside of a cylinder. We consider first film dynamics in a horizontal tube (Sec. 3). We identify a capillary equilibrium not described by previous authors (which we term the *dry spot*) and determine the stability of this and other equilibrium solutions; we extend Jensen's map of parameter space [13] to smaller Bond numbers where the dry spot arises, and show that it is associated with hysteresis in the transition between rivulets and collars. We then consider briefly the less studied case of a film coating a tilted tube (Sec. 4), the generic situation in applications such as lung airways. Here the transverse component of gravity drives fluid from the upper to the lower side of the tube while the axial component drives fluid down its length. We illustrate the richness of the dynamics and examine how an isolated drop slides down a tilted tube. Somewhat counterintuitively, we find that drops slide most rapidly down tubes that are not vertical.

2 Model

We consider a cylindrical tube of radius a and length L, tilted at an angle α to the horizontal (Figure 1). Gravity g acts vertically downwards. The surface of the tube is parametrized by cylindrical polar coordinates θ and z, where $a\theta$ measures azimuthal distance ($\theta = 0$ is oriented upwards in a vertical plane) and az measures axial distance along ($\alpha = 0$) or below ($\alpha > 0$) the horizontal. The tube is lined with a thin layer of Newtonian liquid of thickness $\epsilon a h(z, \theta, t)$, where $\epsilon \ll 1$ and $h = O(1)$. The liquid has uniform density ρ, surface tension γ and viscosity μ; time t is scaled on $\mu a/\epsilon^3\sigma$. The liquid layer is assumed to be stress free at its free surface and to satisfy no slip at the cylinder. Intermolecular (van der Waals) forces are neglected, consistent with perfect wetting of the cylinder by the liquid.

Lubrication theory [19] then yields the following dimensionless leading-order evolution equation for the film thickness:

$$h_t + \left[\tfrac{1}{3}h^3\left(\left(h + \nabla^2 h\right)_\theta + \delta \sin\theta\cos\alpha\right)\right]_\theta + \left[\tfrac{1}{3}h^3\left(\left(h + \nabla^2 h\right)_z + \delta\sin\alpha\right)\right]_z = 0, \qquad (2.1)$$

where $\delta = \rho g a^2/(\gamma\epsilon) = O(1)$ is a reduced Bond number and subscripts z, θ and t denote derivatives. The azimuthal component of gravity $\delta\cos\alpha\sin\theta$ drives draining flows from the upper to the lower wall of the tube; the axial component $\delta\sin\alpha$ drives fluid down the tube. We neglect $O(\epsilon)$ corrections to this equation, associated for example with hydrostatic pressure variations across the film [16]. For horizontal tubes ($\alpha = 0$) we impose symmetry about $\theta = 0$ and $\theta = \pi$, setting $h_\theta = h_{\theta\theta\theta} = 0$ there, and impose no-flux conditions $h_z = h_{zzz} = 0$ at $z = \pm L/2$. For $\alpha > 0$ we impose instead periodic boundary conditions $h(-L/2, \theta) = h(L/2, \theta)$, $h_z(-L/2, \theta) = h_z(L/2, \theta)$, etc. The dimensionless fluid volume

$$V = \int_{-L/2}^{L/2}\int_0^{2\pi} h\,\mathrm{d}\theta\,\mathrm{d}z \qquad (2.2)$$

is an $O(1)$ quantity that remains constant during the evolution of the film, and solutions of (2.1) are in general parametrized by V, α, δ and L. When $\alpha = 0$, equilibrium solutions of (2.1) may be parametrized by $(L, \mathcal{V})$, where $\mathcal{V} = V/\pi\delta$ [13], because the pressure is linear in h (see for example (3.4) below).

When $\delta = 0$ and $\partial_\theta = 0$, (2.1) reduces to the evolution equation studied in, for example, refs. [1, 3, 4]. The limit $\alpha = 0$, $\delta > 0$ has been considered in refs. [13] (exploiting the fact that, to leading order, substrate curvature in a curved tube has the same effect as gravity in a straight tube) and [16] (who included higher-order terms); the limit $\alpha = \pi/2$, $\partial_\theta = 0$ was considered in, for example, refs. [5, 6, 20]. Full details of the derivation of this class of equation may be found in these earlier works.

When solving (2.1) numerically, we exploited symmetry where possible, working in the domain $0 \leq \theta \leq \pi$ and (when $\alpha = 0$) $0 \leq z \leq L/2$. We used second-order accurate centered finite-difference schemes to discretize the spatial derivatives in (2.1), keeping the time derivative continuous. The grid used $M \times N$ points in (z, θ). The spatial discretization was done using either a 21-point stencil or a 13-point stencil [21]. The resulting system of coupled ODEs were solved using the multistep implicit schemes DDASSL (when applying no-flux conditions, requiring inversion of a banded matrix) and DASPK (when periodic conditions were applied, requiring inversion of a sparse matrix) from the SLATEC library [22]. Typically we used $M = 101$, $N = 51$, using grid refinement where necessary to ensure accuracy. Solutions were validated against independent one-dimensional codes [4, 13, 23] and against exact and asymptotic results (see below). In all our simulations h remained strictly positive, ensuring that singularities associated with moving contact lines were avoided.

For a horizontal tube, we either used the initial condition

$$h(z, \theta, 0) = 1 + \tfrac{1}{2} \cos(\pi z/L) \cos\theta, \tag{2.3}$$

or alternatively continuation methods, whereby the final film configuration from one simulation was used as the initial condition for a new simulation with slightly different parameter values.

3 Horizontal tubes

At large times, in a horizontal tube, fluid accumulates in equilibria with zero effective contact angle, surrounded by regions in which $h \to 0$ as $t \to \infty$ (e.g. a thinning lobe between two collars). We denote such regions as "dry," although there is no mechanism for finite-time film rupture within the present model.

We classify possible equilibrium solutions using the scheme shown in Figure 2. A *drop* (D) is an isolated dome of fluid that sits at the bottom of the tube. A localized annular collar can either be axisymmetric (AC), as described by Hammond [1], or non-axisymmetric (NAC) [16]. A rivulet can either be uniform (UR) or wavy (WR), coating the bottom of the tube and having a straight or wavy effective contact line respectively [13]. A *dry spot* (DS) is an isolated region along the top of the tube in an otherwise completely coated tube that has near-zero fluid thickness. The symmetry of all these solutions under reflections in $\theta = \pi$ and $z = 0$ requires us to compute only in the square ABDC, where A$= (0, 0)$, B$= (0, \pi)$, C$= (L/2, 0)$, and D$= (L/2, \pi)$. We denote the fluid height at these corners by h_{A}, h_{B}, etc. While solutions of the type WR, UR, D, AC and

NAC have been described previously in this context [1, 13, 16, 17], to the best of our knowledge dry spots have not.

3.1 The effect of increasing gravity

Figure 3 shows the effect of increasing δ in a domain of length $L = 3\pi$, whereby a collar becomes a rivulet. The fluid has fixed volume $V = 6\pi^2$ in these simulations, so that $\mathcal{V} = V/\pi\delta$ decreases. For $\delta = 0$ we find that a stable axisymmetric collar forms as $t \to \infty$. It has width 2π and is centered on $z = 0$, with thinning lobes in $\pi < |z| < 3\pi/2$. The fluid heights at the collar's effective contact line (along $z = \pi$) and at corners C and D decay with $h \sim t^{-1/2}$ and $t^{-1/4}$ respectively, consistent with [1]. Increasing gravity slightly ($0 < \delta \lesssim 0.6$) causes a loss of symmetry, and the collar becomes nonaxisymmetric (Figure 3(a)), becoming deeper and longer along the base of the tube (so that $h_{\rm A} < h_{\rm B}$, Figure 3(e)). Increasing the Bond number further ($0.6 \lesssim \delta \lesssim 1.3$) turns the collar into an isolated drop (Figure 3(b)), for which $h_{\rm A}$, $h_{\rm C}$ and $h_{\rm D} \to 0$ as $t \to \infty$ (figure 3(e)). Increasing the Bond number to $1.3 \lesssim \delta \lesssim 2.65$ causes the drop to elongate axially until it reaches the domain boundaries, becoming a wavy rivulet (Figure 3(c)), with $0 < h_{\rm D} < h_{\rm B}$ (figure 3(e)). For $\delta \gtrsim 2.65$ the rivulet becomes axially uniform (Figure 3(d)). Simulations in this case starting from (2.3) exhibited two distinct decay rates towards the equilibrium, as reported in [13], with the film thickness at the rivulet's effective contact line satisfying first $h_{min} \sim t^{-1/2}$ and later $h_{min} \sim t^{-3/5}$, as different physical effects drive film drainage. The computed WR/UR transition at $\delta \approx 2.65$ ($\mathcal{V} \approx 7.113$) is in excellent agreement with the value $\mathcal{V} \approx 7.114$ predicted using a linear stability analysis in [13].

To recall briefly, this threshold is determined as follows. Static equilibrium solutions of (2.1) satisfy $h = 0$ or $h \geq 0$ with uniform pressure, $h + \nabla^2 h - \delta\cos\theta = -P$. The uniform rivulet $h = h_U(\theta)$ therefore satisfies $h_U + h_{U\theta\theta} - \delta\cos\theta = -P_U$ in $\theta_0 \leq \theta \leq \pi$, for some constant P_U, with $h_{U\theta}(\pi) = 0$ and $h_U = h_{U\theta} = 0$ at the contact line $\theta = \theta_0$. Its location is determined uniquely according to

$$\frac{\pi\mathcal{V}}{L} = \frac{(\pi-\theta_0)^2}{\sin\theta_0} - (\pi-\theta_0)\cos\theta_0 - 2\sin\theta_0. \tag{3.1}$$

To the uniform rivulet one can add a wavy pertubation of the form $h = h_U(\theta) + h_W(\theta)\cos(2\pi z/L)$, and seek conditions under which the branch of WR solutions bifurcates from the UR solution. Linearising about the uniform state yields the eigenvalue problem $(1 - (4\pi^2/L^2))\, h_W + h_{W\theta\theta} = 0$ in $\theta_0 \leq \theta \leq \pi$. The symmetry boundary condition $h_{W\theta}(\pi) = 0$ implies

$$h_W = A\cos\left[\left(1 - \frac{4\pi^2}{L^2}\right)^{1/2}(\pi-\theta)\right] \tag{3.2}$$

for some amplitude $A \ll 1$. The contact line condition $h_W(\theta_0) = 0$ then demands that

$$\left(1 - \frac{4\pi^2}{L^2}\right)\left(1 - \frac{\theta_0}{\pi}\right)^2 = \frac{1}{4}, \tag{3.3}$$

implying that rivulets with $0 \leq \theta_0 < \frac{1}{2}\pi$ are unstable in sufficiently long tubes (with length at least $4\pi/\sqrt{3}$). Thus in the example shown in Figure 3, with $L = 3\pi$, uniform rivulets with $\theta_0 > 0.329\pi$ are stable.

3.2 Non-axisymmetric collars

The structure of non-axisymmetric collars can be captured by a regular asymptotic expansion, which we now summarize briefly. For $\delta \ll 1$ and $\alpha = 0$, a good approximation for a non-axisymmetric collar can be obtained as a perturbation of an axisymmetric collar. In equilibrium, (2.1) implies

$$\nabla^2 h + h - \delta \cos\theta = K \quad \text{or} \quad h = 0 \tag{3.4}$$

where K is a constant (proportional to the uniform pressure in the collar). Symmetry conditions $h_\theta = 0$ apply at $\theta = 0$ and $\theta = \pi$ and $h_z = 0$ at $z = 0$. Along the collar's effective contact line $z = \mathcal{C}(\theta)$, say, $h = 0$ and $\mathbf{n} \cdot \nabla h = 0$, where $\mathbf{n}$ is the unit normal to $\mathcal{C}$ (Figure 2(c)). The volume of the collar in the domain ABDC (Figure 2), namely $\hat{V} = V/4$, is prescribed. Expanding h, $\mathcal{C}$ and K in the form

$$h = h_0(z,\theta) + \delta h_1(z,\theta) + \delta^2 h_2(z,\theta) + \delta^3 h_3(z,\theta) + O(\delta^4) \tag{3.5}$$

yields a series of problems at each order. After careful expansion of boundary conditions and integrals, and extensive algebra (following [13]; see [23] for full details), we find that

$$\begin{aligned} h = \frac{\hat{V}}{\pi^2}(1+\cos z) + \delta\left\{\frac{(z^2-\pi^2)}{2}\cos\theta\right\} + \delta^2\left\{\frac{\pi^4\cosh\sqrt{3}z}{4\hat{V}\cosh\pi\sqrt{3}}\cos 2\theta - \frac{\pi^4}{4\hat{V}}\cos z\right\} \\ + \delta^3\left\{\frac{\pi^6}{8\hat{V}^2}\left(\frac{[M-1]}{\cosh(\pi\sqrt{8})}\cosh(\sqrt{8}z)\cos 3\theta + [M-1]\cos\theta\right)\right\} + O(\delta^4), \end{aligned} \tag{3.6}$$

where $M = \pi\sqrt{3}\tanh(\pi\sqrt{3})$ and $K = \hat{V}/\pi^2 + o(\delta^3)$. The contact line $z = \mathcal{C}(\theta)$ is

$$\begin{aligned} z = \pi - \delta\frac{\pi^3}{\hat{V}}\cos\theta + \delta^2\left\{\frac{\pi^5}{4\hat{V}^2}\left([2-M]\cos 2\theta + 2\right)\right\} + \\ \delta^3\left\{\left(\frac{\pi^7}{8\hat{V}^3}[M-2] - \frac{\pi^8\sqrt{2}}{4\hat{V}^3}[M-1]\tanh(\pi\sqrt{8}) + \frac{5\pi^9}{6\hat{V}^3}\right)\cos 3\theta \right. \\ \left. + \left(\frac{\pi^7}{8\hat{V}^3}[M-2] - \frac{\pi^7}{2\hat{V}^3} - \frac{\pi^9}{2\hat{V}^3}\right)\cos\theta\right\} + O(\delta^4). \end{aligned} \tag{3.7}$$

Figure 4 shows the fluid heights h_A and h_B computed using (3.6) including terms of order δ, δ^2 and δ^3 (curves are extended into $h < 0$ for visual clarity; physical solutions of course require $h \geq 0$), compared to large-time numerical simulations, for a range of δ and $L = 3\pi$. Agreement is good, extending (at $O(\delta^3)$) as far as the NAC/D transition near $\delta = 0.6$ at which $h_\mathrm{A} \to 0$.

3.3 The effect of increasing domain length

Figure 5 shows representative film heights as a function of domain length for fixed fluid volume and Bond number (with $\mathcal{V} = 60$), for which the stability boundary between uniform and wavy rivulets is $L \approx 7.53$ [13]. We obtained solutions via three different approaches: integrating from the default initial condition (2.3) (Figure 5(a)); increasing L incrementally, using the final state of each simulation as the initial condition for the following simulation (Figure 5(b)); and decreasing L incrementally (Figure 5(c)), again

using continuation. Solutions were run until $t = 10^4$ in all cases. These methods reveal the existence of multiple equilibrium solutions and significant transient effects.

Figure 5(a) shows three distinct solutions: uniform rivulets up to the predicted stability boundary; a short window of (apparently stable) wavy rivulets; and non-axisymmetric collars for sufficiently large L. Under forward continuation (Figure 5(b)) the width of the *WR* window is larger but the waviness of the rivulet's contact line is of smaller amplitude than in Figure 5(a). Because growth-rates are small near bifurcation points, we infer that the small-amplitude wavy rivulets in Figure 5(b) are transient (denoted *TWR*): by $t = 10^4$ they have not yet escaped from the nearby unsteady *UR* solution to saturate as the equilibrium *WR* or *NAC* solutions captured in Figure 5(a).

A new type of transient solution was identified when using the method of forward continuation: the dry spot (*DS*, Figure 2(f)). As illustrated by the simulation in Figure 6(a), over a range of times ($t_1 < t < t_2$), the solution domain has three wetted corners and one corner having a height very close to zero. This example arose close to the *WR*/*NAC* boundary; the *WR* solution for $L/2 = 3.86$ was used as the initial condition in a domain of length $L/2 = 3.87$. In this case, the dry spot arose only transiently. In contrast, using backward continuation from the *NAC* solution branch (Figure 5(c)), dry-spot solutions were obtained that persisted for long times and therefore appear to be stable equilibria (see Figure 6(b)). Further reductions in length again yielded *TWR* solutions (Figure 5(c)); in this example, the *TWR* solutions are still approaching the nearby stable *UR* solution at $t = 10^4$.

Figure 7(a) is a sketch of what we infer the equilibrium solution structure to be for $\mathcal{V} = 60$, using the apparent equilibrium values for h_{B} in Figures 5. Hysteresis is evident. The transient dry spot shown in Figure 6 arises near the right-hand fold F, in passing from the *WR* to *NAC* branches. This transition is to be anticipated on topological grounds, assuming the shape of the contact line evolves continuously. We assume that, somewhere along the unstable solution branch between the two folds (shown dashed in Figure 7(a)), equilibria change smoothly from *WR* to *DS*.

3.4 Parameter space

We can now construct a picture of $(L, \mathcal{V})$-parameter space (Figure 7(b)). Much of the structure was identified previously (see figure 8 of ref. [13]), particularly the *UR*/*WR* and *WR*/*D* boundaries and the transition to rivulets with two or more waves in the solution domain (not shown). While Jensen [13] showed that the *UR*→*WR* transition is supercritical for large $\mathcal{V}$, he did not compute the *WR*/*D* boundary for $\mathcal{V} > 12$ (and thus not the full transition shown in Figure 3(e)). We propose in Figure 7(b) a possible extension to the existing map of parameter space for large $\mathcal{V}$ that includes the *D*/*NAC* boundary (well approximated by setting $h_{\mathrm{A}} = 0$ in (3.6); this boundary lies above $\mathcal{V} = 30$). The transition *NAC*→*D*→*WR*→*UR* in Figure 3(e) is shown with a vertical arrow in Figure 7(b). Based on the inferred bifurcation structure in Figure 7(a), and the topological requirement that a continuous *WR*→*NAC* transition can only occur at a codimension-2 bifurcation point, we postulate a likely structure of parameter space for large $\mathcal{V} = V/\pi\delta$, notably that the folds F originate from the intersection point of the *NAC*/*D* and *WR*/*D* boundaries. The expense of unsteady computations prevented us from using the present methods to map out all these boundaries in detail; further work is required to confirm these predictions.

4 Tilted tubes

We now tilt the tube (setting $\alpha > 0$ in (2.1)) and impose periodic boundary conditions in z. Figure 8 demonstrates the richness of the film's dynamics. Using the axially uniform rivulet shown in Figure 3(d) as an initial condition in a tube of length 12π, we set $\alpha = 11\pi/24$ and $\delta = 0.1$. The initially uniform rivulet becomes wavy at $t \approx 105$ before developing four distinct peaks ($t \approx 120$). These peaks develop into adjacent drops separated by thin connecting films ($t \approx 160$). The drops eventually wrap around the inside of the tube to create non-axisymmetric collars. One of the four drops is swallowed by a neighboring collar just after $t = 220$. At $t = 400$, three non-axisymmetric collars are traveling down the tube. This distribution coarsens to two and ultimately a single collar, with large collars moving faster and ultimately absorbing smaller collars, as reported for vertical tubes [6].

We do not attempt to disentangle all aspects of this behavior (beyond noting that the $UR \rightarrow WR \rightarrow D \rightarrow NAC$ transition in Figure 8 recapitulates the sequence upwards along the vertical arrow in Figure 7(b)), but instead we address one key feature, namely the motion of an isolated drop down a tilted tube.

4.1 Motion of an isolated drop

We now consider an initial profile that consists of a drop of length L_d at one end of the tube, surrounded by a thin precursor layer of thickness $\eta \ll 1$:

$$h(z, \theta, 0) = A(1 + \cos[(1 - 2z/L_d)\,\pi])(1 + \cos[(1 - \theta/\pi)\,\pi]) + \eta. \tag{4.1}$$

Figure 9 shows the evolution of this drop as it flows down a tube with $\alpha = \pi/12$, $\delta = 1$, $L = 12\pi$, $\eta = 0.001$, $A = 1$ and $L_d = 3\pi$. For early times (roughly up to $t = t_3 = 1$) there is no movement of the contact line, but the front of the drop steepens as its maximum increases in height and moves slowly down the tube; this is a form of 'waiting time' behavior. As the drop slides down the tube it loses volume to a thick deposited tail. The profiles shown at $t = 22$ in figure 9 reveal a second maximum that forms in the tail, either via a Rayleigh instability or possibly because the drop moves at an unsteady speed and so deposits a nonuniform film thickness. This second maximum persists but travels at a slower speed than the main body of the drop.

Figure 10 shows profiles of drops at $t = 60$ for a range of tilt angles. For $\alpha \leq \pi/3$, the distance travelled increases with α. However, the drop in the vertical tube ($\alpha = \pi/2$) does not move as far down the tube as either of the drops in the tubes tilted at angles $\alpha = \pi/3$ or $\alpha = \pi/4$, despite having a greater tilt. Tilting the tube reduces the azimuthal gravitational component $\delta \cos\alpha$, allowing the drop to spread around the inside of the tube in the azimuthal direction, so increasing the width of both the drop and its tail. For $\alpha = \pi/2$ this widening has taken place to such an extreme that the tail of the drop completely wraps around the tube's interior. Figure 11 shows in more detail how the drop speed depends on time and governing parameters. Figure 11(a) demonstrates that the slower motion of a drop in a vertical tube (relative to the case $\alpha = \pi/3$) is sustained over long times; the effect is exaggerated by increasing the Bond number (Figure 11(b)) and drop volume (Figure 11(d)). Increasing the precursor film thickness to $\eta = 0.01$ has marginal effect; increasing by a further order of magnitude (Figure 11(c)) increases drop speeds but again causes drops in vertical tubes to fall increasingly slowly compared

to tilted tubes. We infer that the drop dynamics are controlled by a balance between dissipation at the advancing contact line and release of potential energy (as in [5, 10]), so that wider drops are subject to greater dissipation and therefore travel slower. (In the most extreme case, $\alpha = \pi/2$ in figure 11(d), the front of the drop wraps entirely around the interior of the tube to become a collar for $t \gtrsim 8$.) Additional factors complicate this picture, notably reduction in drop volume by formation of a thick tail, and the dependence of drop width on drop volume and tilt angle. These factors combine to make speed a non-monotonic function of tilt angle.

5 Discussion

We have used simulations of an evolution equation derived from lubrication theory to describe the behavior of films coating horizontal and tilted tubes. We have neglected numerous physical effects that could influence such films, notably tube rotation, shear stresses from external or internal flows, finite film-thickness effects that might lead to drop or liquid-bridge formation, inertia, surfactants, substrate compliance, film rupture, and so on. Even so, the competition between surface tension, gravity and viscous forces yields a dynamical system of considerable complexity.

In horizontal tubes, we have extended the existing description of parameter space for equilibrium solutions [13] to include the transitions between non-axisymmetric collars and rivulets as gravity is increased (Figure 3), between non-axisymmetric collars and uniform rivulets as tube length is decreased (which exhibits hysteresis, Figure 5) and we have identified a new equilibrium solution (the dry spot) which arises at very low Bond numbers. Our transient simulations were obviously not able to capture unstable solution branches, and we also needed to interpret carefully results in the neighborhood of near-neutrally-stable equilibria (Figure 5). Direct computation of equilibria as a free-boundary problem is a valuable complementary approach that we used to characterize non-axisymmetric collars (Section 3.2).

In a tube tilted to the vertical, axial and azimuthal draining flows compete with the Plateau–Rayleigh instability (Figure 8) to allow dynamic transitions between rivulets and collars. We showed how the speed of an isolated drop is non-monotonic in tilt angle, while being strongly influenced by losing volume to a thick deposited tail (similar to that of a wetting drop on a vertical wall [24]). We also found in our simulations that axial flows may promote rivulet stability [23]; we will report on this feature elsewhere. The evolution of thin films coating tilted tubes at low Bond numbers has received remarkably little attention from experimentalists and we hope that this preliminary study will motivate future work in this area.

Finally, it is worth noting some of the physiological implications of our findings. In horizontal tubes, uniform films of thin, Newtonian wetting films drain to form spatially non-uniform structures, be they rivulets, collars, drops or even dry spots (Figure 7(b)). In tilted tubes also, rivulets or collars appear to be generic (Figure 8). This implies that additional factors are required to ensure a relatively uniform coating of lung airways, such as homeostatic fluid balance by the underlying epithelium, non-Newtonian effects such as mucus yield stress and active transport by cilia. Non-uniformly distributed films, such as those we have computed here, will have a critical bearing on the the protective capacity of the airway liquid lining, and on the efficiency of drug-delivery therapies relying on

Marangoni effects [25].

Acknowledgements

This work was supported by an EPSRC studentship. We acknowledge several helpful conversations with Dr Rachel Levy.

References

[1] P. S. Hammond. Nonlinear adjustment of a thin annular film of viscous fluid surrounding a thread of another within a circular pipe. *J. Fluid Mech.*, 137:363–384, 1983.

[2] F. Mashayek and N. Ashgriz Instability of liquid coatings on cylindrical surfaces. *Phys. Fluids*, 7:2143–2153, 1995.

[3] S. G. Yiantsios and B. G. Higgins. Rayleigh-Taylor instabilities in thin viscous films. *Phys. Fluids*, 1:1484–1501, 1989.

[4] J. R. Lister, J. M. Rallison, A. A. King, L. J. Cummings, and O. E. Jensen. Capillary drainage of an annular film: the dynamics of collars and lobes. *J. Fluid Mech.*, 552:311-343, 2006.

[5] S. Kalliadasis and H. C. Chang. Drop formation during the coating of vertical fibres. *J. Fluid Mech.*, 261:135–168, 1994.

[6] V. I. Kerchman and A. L. Frenkel Interactions of coherent structures in a film flow: Simulations of a highly nonlinear evolution equation. *Theor. Comput. Fluid Dyn.*, 6:235–254, 1994.

[7] H. C. Chang and E. A. Demekhin. Mechanism for drop formation on a coated vertical fibre. *J. Fluid Mech.*, 380:233–255, 1999.

[8] I. L. Klialkhandler, S. H. Davis and S. G. Bankoff Viscous beads on vertical fibre *J. Fluid Mech.*, 429:381–390, 2001.

[9] P. A. Gauglitz and C. J. Radke. An extended evolution equation for liquid film breakup in cylindrical capillaries. *Chem. Eng. Sci.*, 43:1457–1465, 1988.

[10] O. E. Jensen. Draining collars and lenses in liquid lined vertical tubes. *J. Colloid Interface Sci.*, 221:38–49, 2000.

[11] A. L. Frenkel, A. J. Babchin, B. G. Levich, T. Shlang and G. I. Sivashinsky Annular flows can keep unstable films from breakup: Nonlinear saturation of capillary instability. *J. Colloid Interface Sci.*, 115:225–233, 1987.

[12] D. Quéré. Thin films flowing on vertical fibres. *Europhys. Lett.*, 13:721–726, 1990.

[13] O. E. Jensen. The thin liquid lining of a weakly curved cylindrical tube. *J. Fluid Mech.*, 331:373–403, 1997.

[14] B. Reisfeld and S. G. Bankoff Non-isothermal flow of a liquid film on a horizontal cylinder *J. Fluid Mech.*, 236:167–196, 1992.

[15] R. V. Roy, A. J. Roberts & M. E. Simpson. A lubrication model of coating flows over a curved substrate in space *J. Fluid Mech.*, 454:235–261, 2002.

[16] D. E. Weidner, L. W. Schwartz, and M. H. Eres. Simulation of coating layer evolution and drop formation on horizontal cylinders. *J. Colloid Interface Sci.*, 187:243–258, 1997.

[17] J. R. de Bruyn. Crossover between surface tension and gravity-driven instabilities of a thin fluid layer on a horizontal cylinder. *Phys. Fluids*, 9:1599–1605, 1997.

[18] V. Duclaux, C. Clanet and D. Quéré The effects of gravity on the capillary instability in tubes *J. Fluid Mech.*, 556:217–226, 2006.

[19] A. Oron, S. H. Davis, and S. G. Bankoff. Long-scale evolution of thin liquid films. *Rev. Mod. Phys.*, 69:931–979, 1997.

[20] A. L. Frenkel On evolution equations for thin films flowing down solid surfaces. *Phys. Fluids. A*, 5:2342–2347, 1993.

[21] J. A. Diaz and L. Kondic Computing three-dimensional thin film flows including contact lines *J. Comput. Phys.*, 183:274–306, 2002.

[22] S. Li and L. Petzold Design of new DASPK for sensitivity analysis, Technical Report TRCS99-28, University of California at Santa Barbara, Santa Barbara, CA, 1999.

[23] A. A. King, Ph.D. Thesis, University of Nottingham, 2005.

[24] L. W. Schwartz. Viscous flows down an inclined plane: instability and finger formation. *Phys. Fluids A*, 1:443–445, 1987.

[25] H. A. R. Williams and O. E. Jensen Surfactant transport over airway liquid lining of nonuniform depth. *J. Biomech. Eng.*, 122:159–165, 2000.

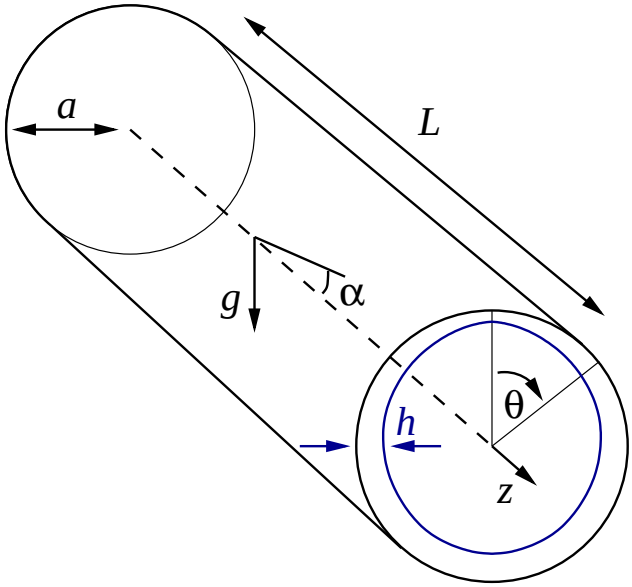

Figure 1: Sketch of the problem: a thin film coats a cylindrical tube, tilted with its axis at an angle α to the horizontal and coated on its interior with a thin liquid film.

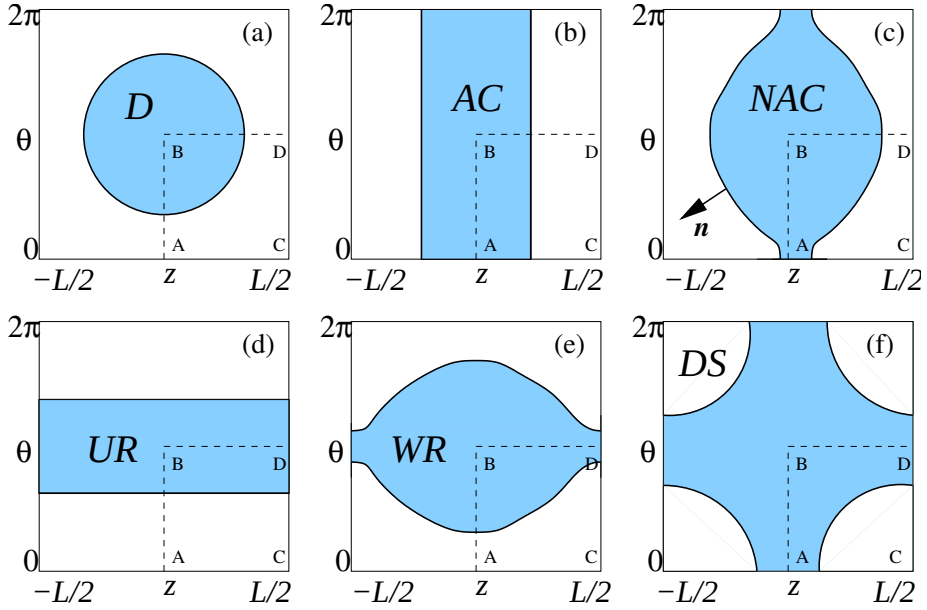

Figure 2: Sketches of possible equilibria in a horizontal tube: (a) drop (D), (b) axisymmetric collar (AC), (c) nonaxisymmetric collar (NAC), (d) uniform rivulet (UR), (e) wavy rivulet (WR) and (f) dry spot (DS). The rectangle with corners A, B, C, D shows the computational domain.

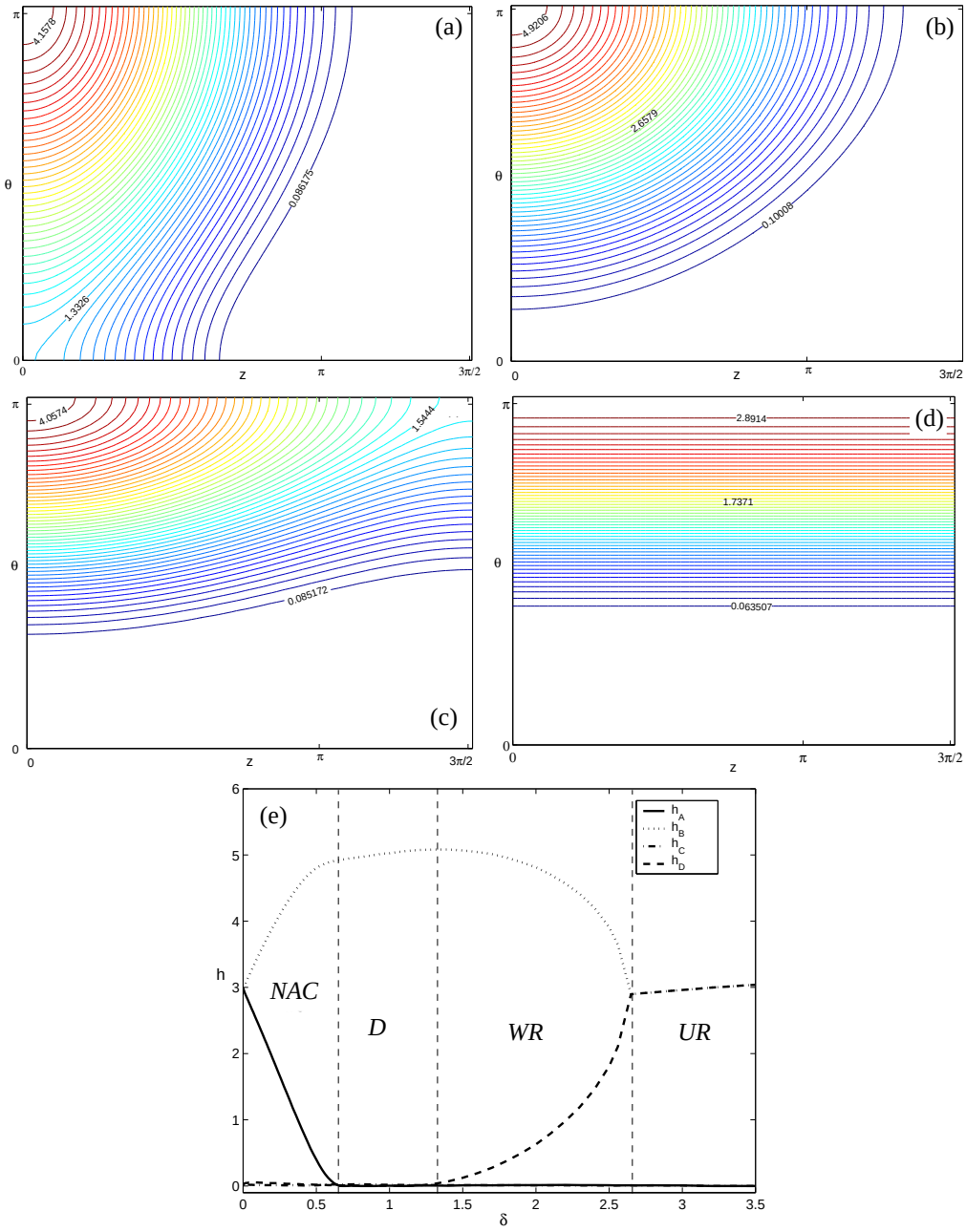

Figure 3: Large-time near-equilibrium solutions of (2.1) for $\alpha = 0$: (a) a non-axisymmetric collar ($\delta = 0.3$, $\mathcal{V} \approx 62.8$) at $t = 10^4$; (b) a drop ($\delta = 1$, $\mathcal{V} \approx 18.8$) at $t = 10^4$; (c) a wavy rivulet ($\delta = 2.4$, $\mathcal{V} \approx 7.9$) at $t = 9 \times 10^3$; (d) a uniform rivulet ($\delta = 3$, $\mathcal{V} \approx 6.3$) at $t = 10^4$. (e) Corresponding corner heights from late-time solutions.

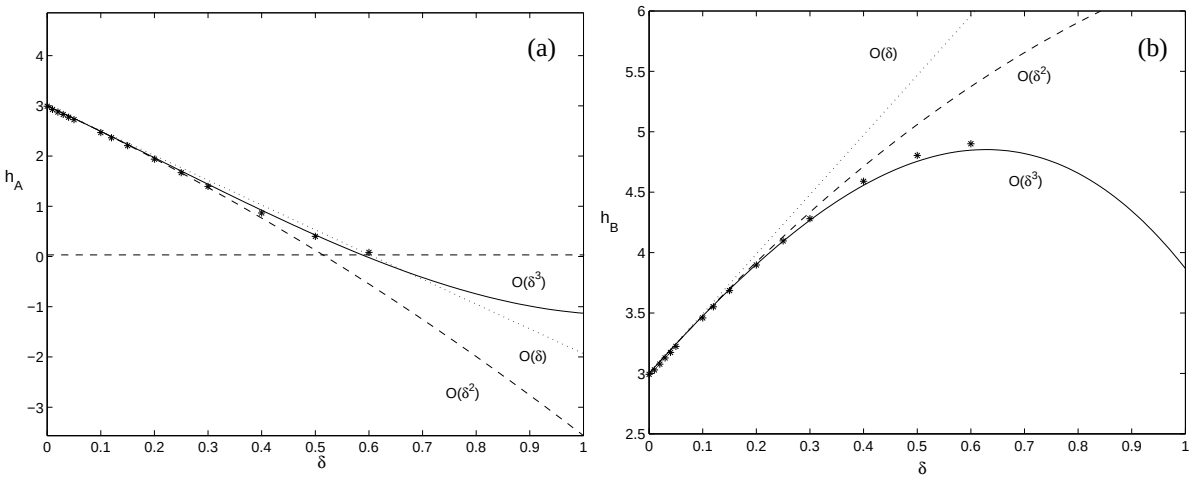

Figure 4: Comparison between (a) $h_{\rm A}$ and (b) $h_{\rm B}$ from (3.6) retaining terms in powers of δ (lines: up to $O(\delta)$ dotted; up to $O(\delta^2)$ dashed; up to $O(\delta^3)$ solid) and determined numerically at $t = 10^4$ (symbols) with $L = 3\pi$ and $\hat{V} = 3\pi^2/2$ (as in Figure 3(e), NAC).

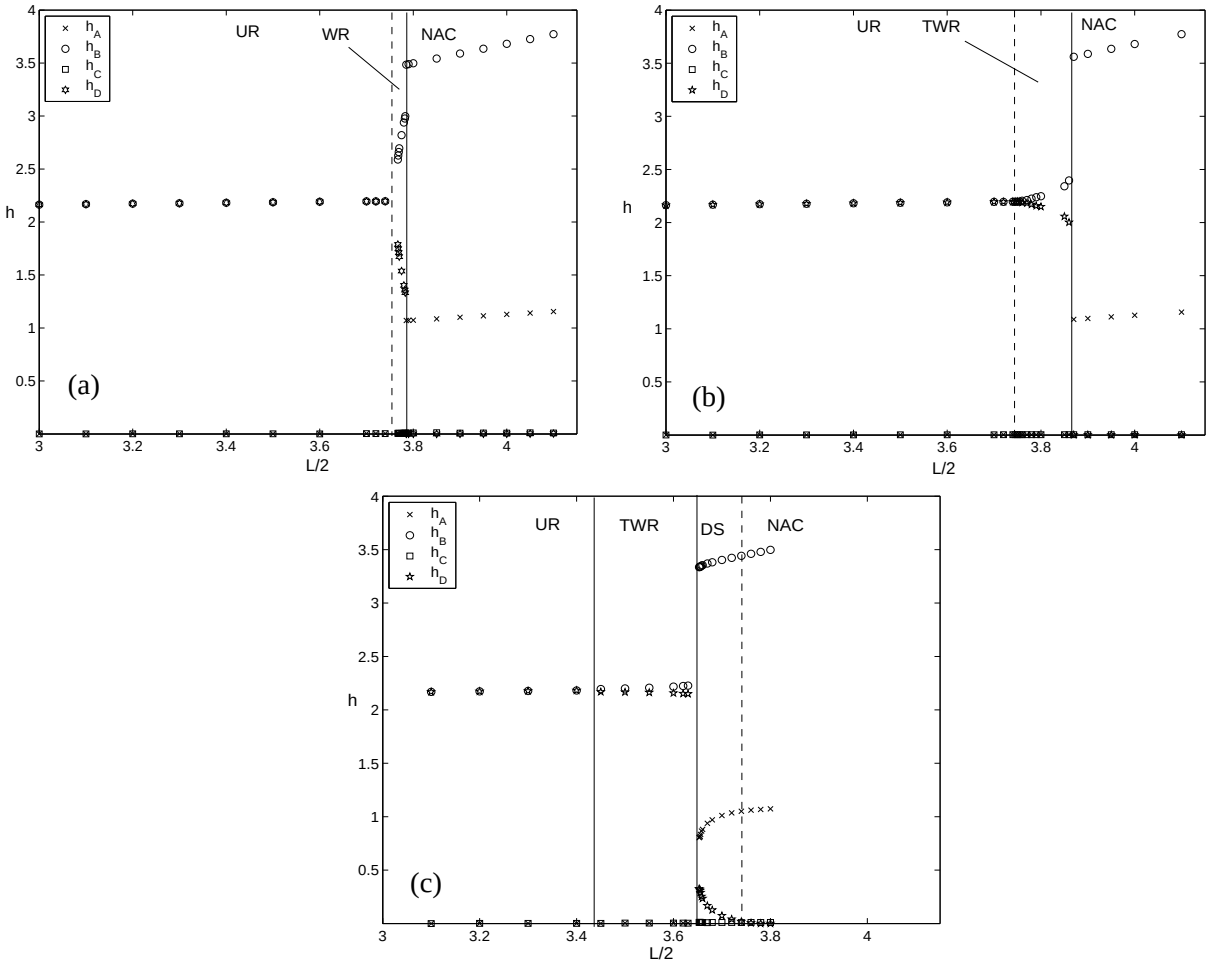

Figure 5: Corner heights at $t = 10^4$ with $\mathcal{V} = 60$, $\alpha = 0$. The initial condition used for (a) is the default profile (2.3); (b) uses forward continuation in L and (c) backward continuation. The solid vertical lines are visual guides; the dashed line shows $L/2 \approx 3.76$, the *UR/WR* linear stability boundary (from [13]).

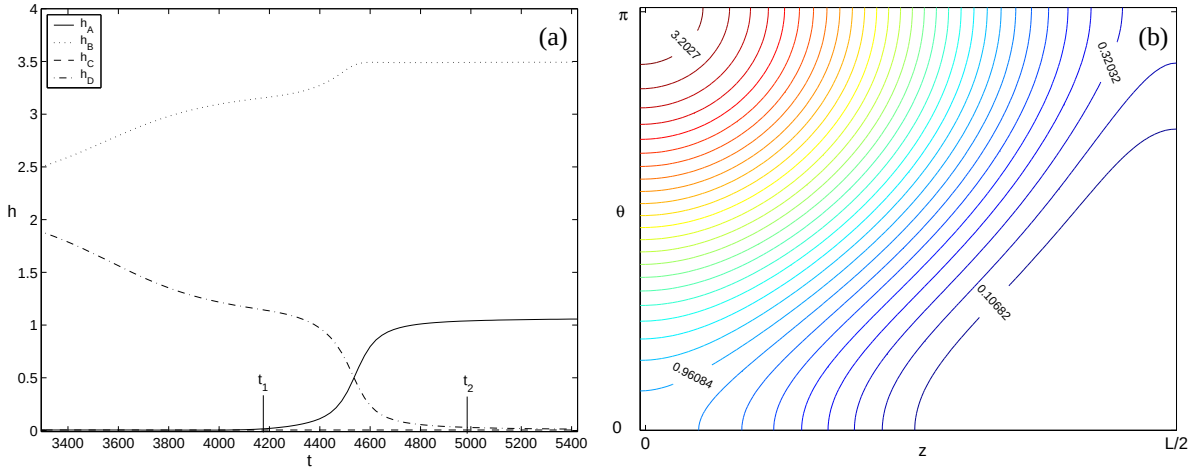

Figure 6: (a) The corner heights of the fluid profile calculated using forward continuation with $L/2 = 3.87$ and a WR initial condition. The calculated long-time stable solution is a non-axisymmetric collar. For $t < t_1$ the solution profile is of wavy rivulet form and for $t > t_2$ the solution resembles a non-axisymmetric collar. Between t_1 and t_2 the solution profile is a transient dry spot. (b) The stable dry spot solution for $L/2 = 3.64$. The initial profile used was the equilibrium NAC calculated using a domain length of $L/2 = 3.65$.

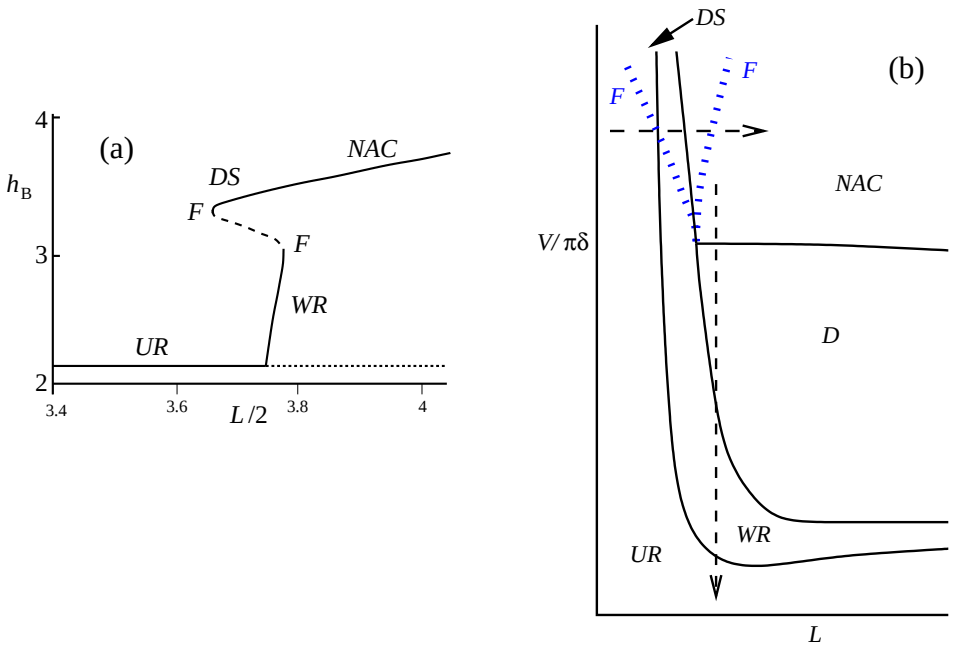

Figure 7: (a) A sketch of the inferred steady solution structure, plotting corner height h_B for $\mathcal{V} = 60$, $\alpha = 0$; solid lines indicate stable and dashed unstable equilibria; folds are denoted F. Solid lines are constructed from numerical data in Figure 5; the dashed line is inferred. (b) A sketch of $(L, \mathcal{V})$-parameter space. The vertical arrow corresponds to figure 3(e) and the horizontal arrow to panel (a).

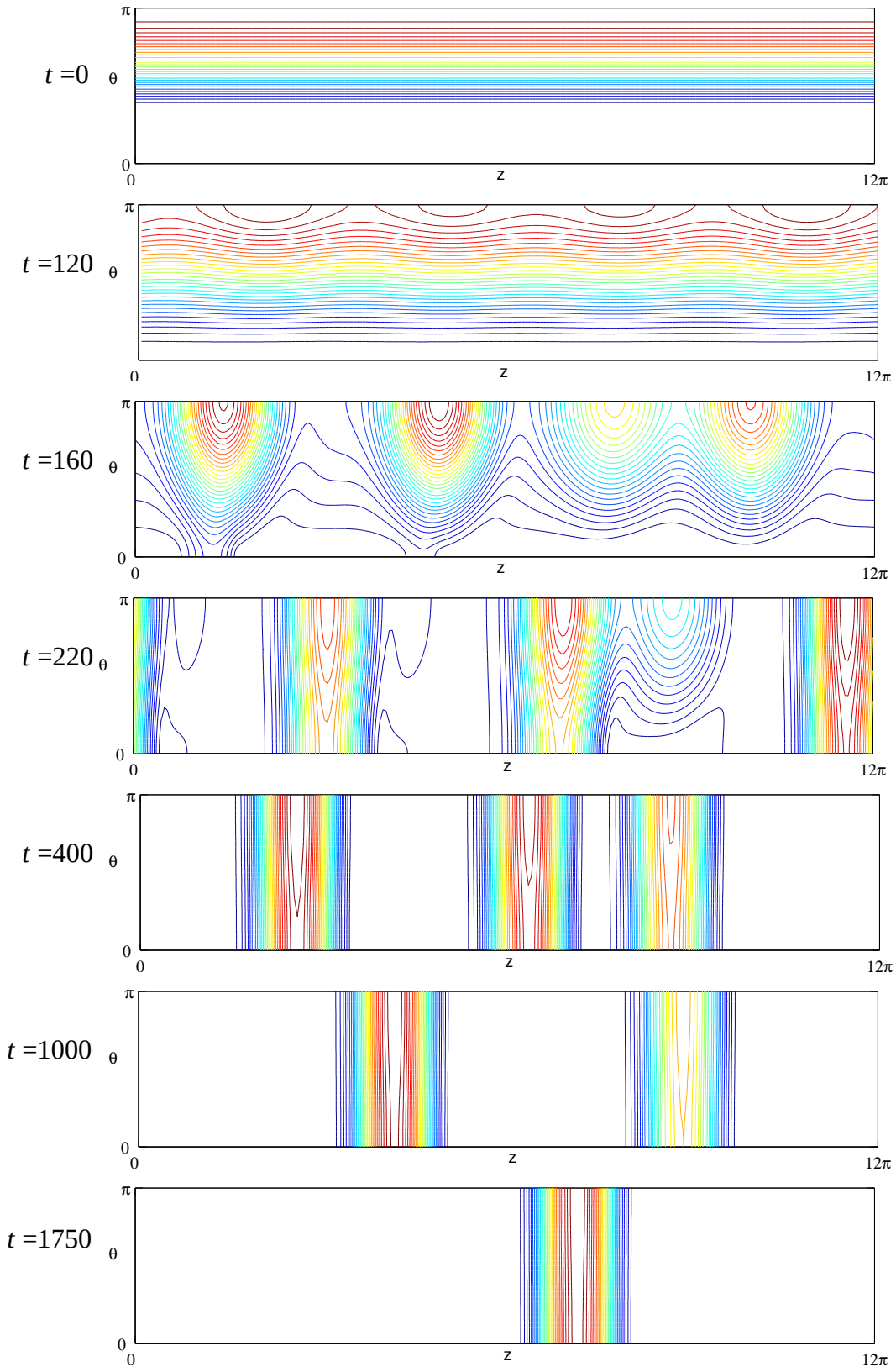

Figure 8: Transition from rivulet to collar in a tube tilted at $\alpha = 11\pi/24$ with $\delta = 0.1$ and $L = 12\pi$, at times shown. The dominant flow is from left to right.

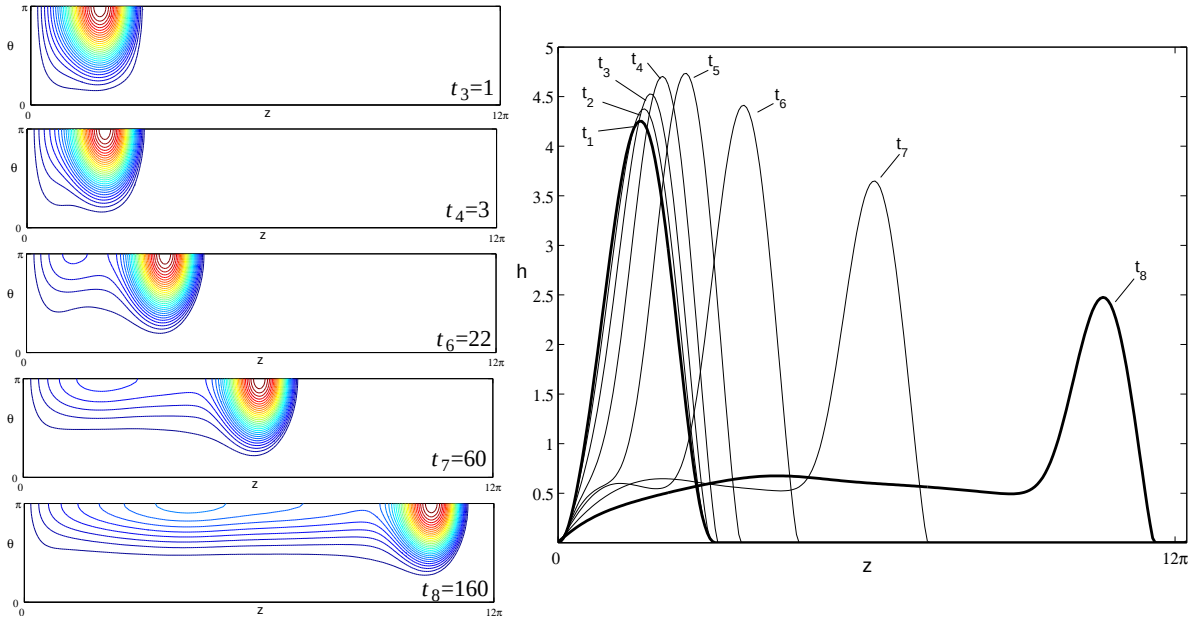

Figure 9: Contour plots (left) and axial profiles along $\theta = \pi$ (right) of a drop of fluid in a tilted tube, with $\alpha = \pi/12$, $\delta = 1$, $L = 12\pi$ and $\eta = 0.001$ at times $t_1 = 0$, $t_2 = 0.15$, $t_3 = 1$, $t_4 = 3$, $t_5 = 8$, $t_6 = 22$, $t_7 = 60$ and $t_8 = 160$.

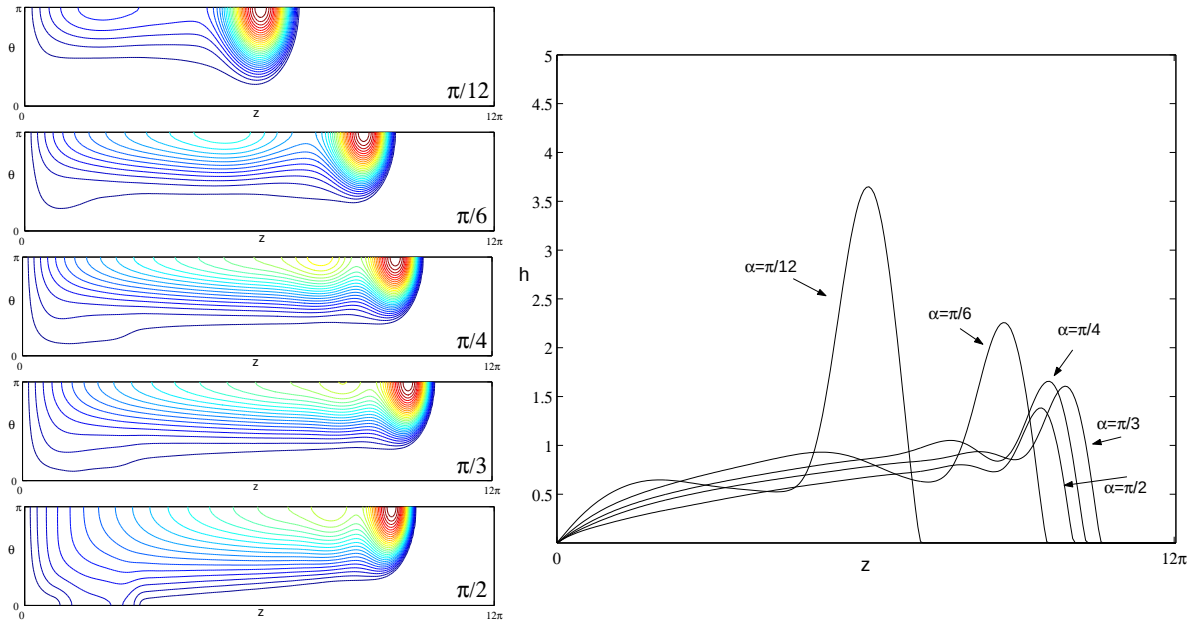

Figure 10: Contour plots (left) and axial profiles along $\theta = 0$ (right) of the profile of a drop of fluid sliding down a tube with $\delta = 1$, $\eta = 0.001$ and $L = 12\pi$ for angles α as shown at $t = 60$.

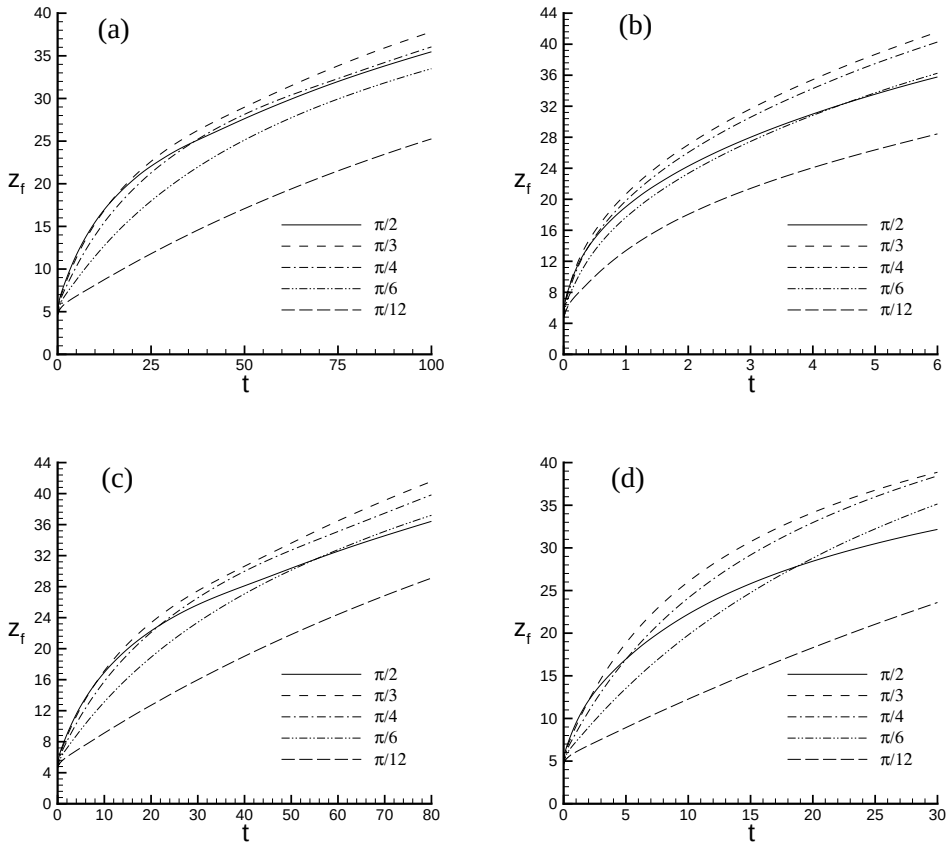

Figure 11: Leading edge location z_f of the advancing drop, plotted versus time for different values of α as indicated. (a) shows baseline case $\delta = 1$, $\eta = 0.001$, $L = 14\pi$, $L_d = 3\pi$, $A = 1$. Parameters are varied individually from baseline as follows: (b) $\delta = 10$; (c) $\eta = 0.1$; (d) $A = 2$.